# The Superconducting Copper Oxychromate $Tl_3(CrO_4)Sr_8Cu_4O_{16}$: Long-Range Ordering between Thallium and Chromium

C. Martin,* F. Letouzé, A. Maignan, R. Seshadri,† C. Michel, M. Hervieu, and B. Raveau

*Laboratoire Crismat, CNRS URA 1318, ISMRA et Université de Caen, Bd du Maréchal Juin 14050 Caen Cedex, France*

*Received October 9, 1995. Revised Manuscript Received January 25, 1996*⊗

Long-range ordering between chromium and thallium has been evidenced for the first time in the copper oxychromate $Tl_3(CrO_4)Sr_8Cu_4O_{16}$ using HREM and XRD. This compound, which crystallizes in an orthorhombic cell with $a = 3.778$ (1) Å, $b = 15.244$ (1) Å, and $c = 17.677$ (1) Å, derives from the "1201" $TlSr_2CuO_5$ structure, by replacing one row of Tl atoms out of four by one row of chromate groups in an ordered way. This superconductor, whose $T_c$(onset) can be raised to 34 K after argon−hydrogen annealing, exhibits a rather high superconducting volume fraction (>40%) compared to other "1201" thallium cuprates. Doping with lanthanum destroys the long-range ordering and weakens superconductivity. The electron microscopy study of this phase also shows the existence of other local superstructures that are interpreted in terms of various modes of ordering of Tl atoms and $CrO_4$ groups.

## Introduction

Among the numerous layered thallium cuprates, the "1201" oxides exhibit distinct behavior since very few of them are superconductors. The cuprates $TlSr_2CuO_{5-\delta}$[1−3] and $Tl_{1-x}Mo_xSr_2CuO_{5-\delta}$[4] have never shown any signature of superconductivity. In contrast, superconductivity below 40 K has been observed in the cuprates $Tl_{0.5}Bi_{0.5}Sr_2CuO_{5-\delta}$,[5] and $Tl_{1-x}Pr_xSr_{2-y}Pr_yCuO_{5-\delta}$,[6] but for these compounds, the diamagnetic volume fraction was found to be small (less than 5%). For $Tl_{0.5}Pb_{0.5}Sr_2CuO_{5-\delta}$, different conclusions have been reported: superconductor[7] or not.[8,9] The chromium phase $(Tl,Cr)Sr_2CuO_5$ synthesized by Sheng et al. exhibits a $T_c$ of 40 K and is of interest.[10] Unfortunately neither its exact composition nor its superconducting volume fraction is known. Moreover the examination of the powder X-ray diffraction pattern presented in ref 10 evidences extra peaks that cannot be indexed in the tetragonal cell defined by the authors. Such an observation suggests possible ordering phenomena within the $[(Tl,Cr)O]_\infty$ layers, in agreement with the size and coordination differences that may exist between thallium and chromium. For this reason the system Tl−Cr−Sr−Cu−O has been reinvestigated. We report herein on the long-range ordering that appears between chromium and thallium in this "1201" phase, which can be formulated as the copper oxychromate $Tl_3(CrO_4)Sr_8Cu_4O_{16}$. The influence of substituting lanthanum for strontium upon this phenomenon is also studied.

## Experimental Section

The samples were prepared by solid-state reactions according to the nominal compositions $Tl_{1-x}Cr_xSr_2CuO_z$, varying $x$ from 0.1 to 0.55 in steps of 0.15 using $Tl_2O_3$ and $Cr_2O_3$ in suitable proportions. Different nominal oxygen contents ($4.5 \le z \le 6.5$) were considered for the $x = 0.25$ composition by varying the nature of the starting strontium and copper compounds: $2SrO_2 + CuO$ or $SrO_2 + SrCuO_2$ or $Sr_2CuO_3$. The mixtures were pressed in the form of bars, introduced into alumina crucibles, sealed in evacuated silica tubes, heated at temperatures ranging from 880 to 920 °C for 6 h, and finally quenched to room temperature. Annealings in an $Ar/H_2$ (90%−10%) flow at low temperature (280 °C) were performed in order to improve the superconducting properties.

The samples were systematically analyzed by X-ray diffraction (XRD) and energy dispersive spectrometry (EDS). The data were collected by means of a Philips vertical diffractometer using Cu Kα radiation, in the range $5° \le 2\theta \le 100°$ in steps of 0.02 ($2\theta$). The structure calculations were performed using the Rietveld method (program Fullprof[11]). The electron diffraction (ED) study was carried out with a JEOL 200CX electron microscope fitted with a eucentric goniometer (±60°) and the high-resolution electron microscopy (HREM) with a Topcon 002B microscope having a point resolution of 1.8 Å. Both microscopes were operated at 200 kV and equipped with an EDS analyzer (Kevex). The samples were ground in alcohol and the small crystal fragments deposited on a holey carbon film. Simulated HREM images were calculated using the MacTempas program.

† On leave from the Solid State and Structural Chemistry Unit, Indian Institute of Science, Bangalore 560012, India.

⊗ Abstract published in *Advance ACS Abstracts,* March 1, 1996.

(1) Ganguli, A. K.; Subramanian, M. A. *J. Solid State Chem.* **1991**, *93*, 250.
(2) Ohshima, E.; Kikuchi, M.; Izumi, F.; Hiraga, K.; Oku, T.; Nakajima, S.; Ohnishi, N.; Morii, Y.; Funahashi, S.; Syono, Y. *Physica C* **1994**, *221*, 261.
(3) Kim, J. S.; Swinnea, J. S.; Steinfink, H. *J. Less. Common Met.* **1989**, *156*, 347.
(4) Letouzé, F.; Martin, C.; Maignan, A.; Michel, C.; Hervieu, M.; Raveau, B. *Physica C* **1995**, *254*, 33.
(5) Pan, M. H.; Greenblatt, M. *Physica C* **1991**, *184*, 235.
(6) Bourgault, D.; Martin, C.; Michel, C.; Hervieu, M.; Provost, J.; Raveau, B. *J. Solid State Chem.* **1989**, *78*, 326.
(7) Pan, M. H.; Greenblatt, M. *Physica C* **1991**, *176*, 80.
(8) Martin, C.; Bourgault, D.; Michel, C.; Provost, J.; Hervieu, M.; Raveau, B. *Eur. J. Solid State Inorg. Chem.* **1989**, *26*, 1.
(9) Kwei, G. H.; Shi, J. B.; Ku, H. C. *Physica C* **1991**, *174*, 180.
(10) Sheng, Z. Z.; Li, Y. F.; Tang, Y. Q. ; Chen, Z. Y.; Pederson, D. O. *Solid State Commun.* **1992**, *83*, 205.
(11) Rodriguez-Carvajal, J. *Collected Abstracts of Powder Diffraction Meeting*; Toulouse, France, 1990; p 127.

0897-4756/96/2808-0865$12.00/0 

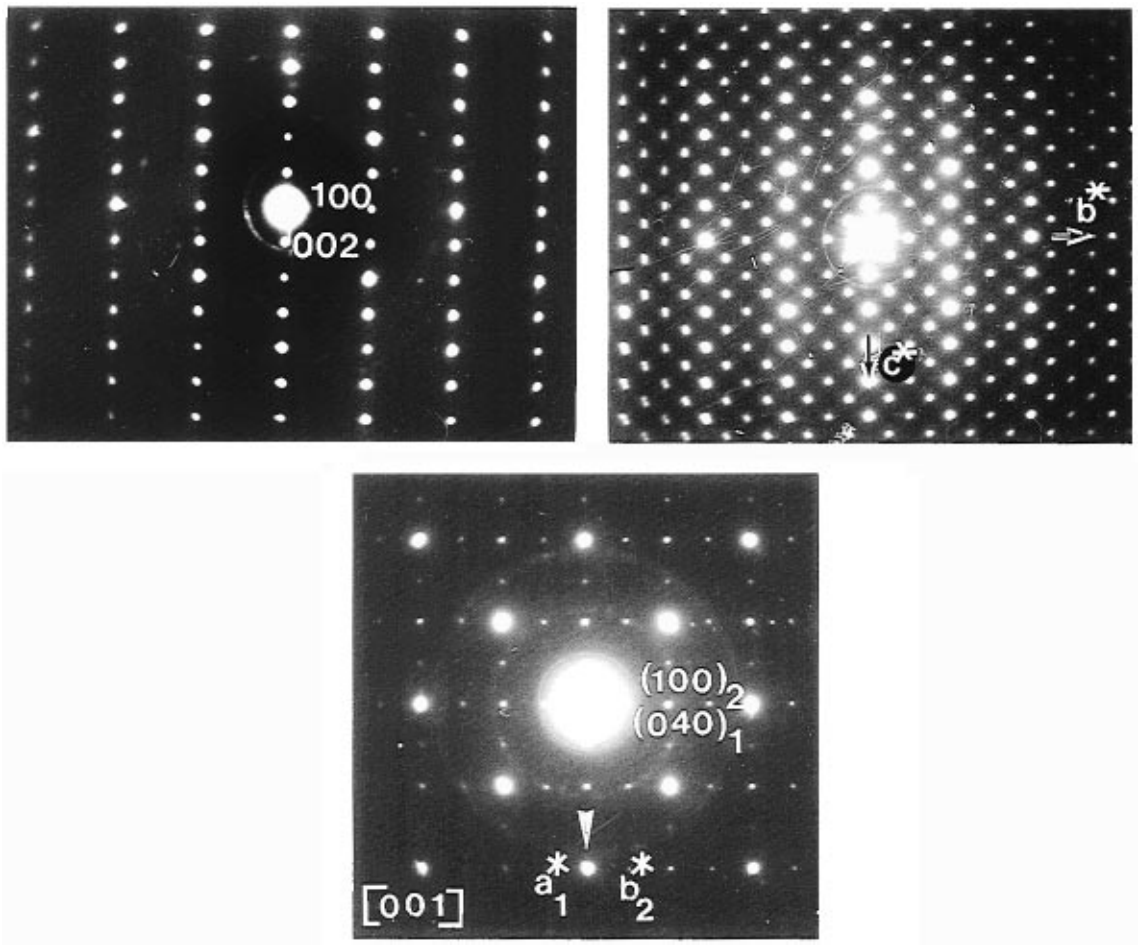


**Figure 1.** ED patterns of the orthorhombic phase $Tl_3(CrO_4)Sr_8Cu_4O_{16}$: (a, top left) [010], (b, top right) [100], and (c, bottom) [001] (note that 90° oriented systems are often observed along this direction, the two components are labeled 1 and 2).

The superconducting properties were studied using a SQUID magnetometer in the range 5 K to $T > T_c$ with an applied field $H = 10$ G. No magnetization corrections were made.

## Results and Discussion

For the above experimental conditions the best results were obtained for the nominal composition $Tl_{3/4}Cr_{1/4}Sr_2CuO_{6.5}$, starting from a mixture of $SrO_2$, CuO, $Tl_2O_3$, and $Cr_2O_3$. Under these conditions, the "1201" phase was obtained practically pure with only traces of $SrCO_3$[12] and $Sr_4Tl_2CO_3O_6$.[13,14] Other attempts lead either to the formation of the oxycarbonate $Tl_{0.7}Cr_{0.3}Sr_4Cu_2CO_3O_7$[15] or to strongly multiphasic samples, especially when the oxygen content was decreased to "$O_{4.5}$".

The EDS analysis performed on numerous crystals confirms that the actual composition is close to the nominal one, "$Tl_{0.7}Cr_{0.3}Sr_2Cu$".

**Evidence for an Orthorhombic Supercell: ED and XRD Study.** The ED study was performed on numerous crystallites of an as-synthesized sample of nominal composition "$Tl_{3/4}Cr_{1/4}Sr_2CuO_{6.5}$". The reconstruction of the reciprocal space confirms that the set of fundamental intense reflections is consistent with the 1201-type structure, i.e., with the subcell $a \approx b \approx a_p$ and $c \approx c_{1201} \approx 9$ Å. However, it evidences two systems of additional reflections.

The first set of rather intense reflections, observed in every crystal of the sample, corresponds to an orthorhombic supercell with

$$a_0 \approx a_{1201} \approx a_p; \qquad b_0 \approx 4a_{1201}; \qquad c_0 \approx 2c_{1201} \approx 18 \text{ Å}$$

The conditions of reflection are $hkl$, $k + l = 2n$, involving A-type symmetry.

The [010], [100], and [001] ED patterns are given in Figure 1a−c, respectively. In the [001] ED patterns (Figure 1c), one often observes the superposition of two 90° oriented systems ($hk0$; $k = 2n$). This is a common feature in such supercells and attests to the superstructure being established along one of the two equivalent directions $[100]_{1201}$ and $[010]_{1201}$ of the 1201 tetragonal subcell. The size of the corresponding domains and the nature of the boundaries will be detailed in the next section.

The second system corresponds to a doubling of the $a_0$ parameter and a loss of the A-type symmetry characterized by weak or very weak additional spots and is observed only in a few crystals. The [001] ED pattern of one such crystal with $a' \approx 2a_0$ ($h + k = 2n$), is given in Figure 2.

The XRD pattern of this phase (Figure 3a) can be indexed in an orthorhombic quadruple cell in agreement with the ED study. Note that the extra reflections that

(12) De Villiers, J. P. R. *Am. Mineral.* **1971**, *56*, 758 .
(13) Schenck, R. V.; Müller-Buschbaum, H. K. *Z. Anorg. Allg. Chem.* **1973**, *396*, 113.
(14) Caignaert, V.; Hervieu, M.; Goutenoire, F.; Raveau, B. *J. Solid State Chem.* **1995**, *116*, 321.
(15) Maignan, A.; Pelloquin, D.; Malo, S.; Michel, C.; Hervieu, M.; Raveau, B. *Physica C* **1995**, *249*, 220.

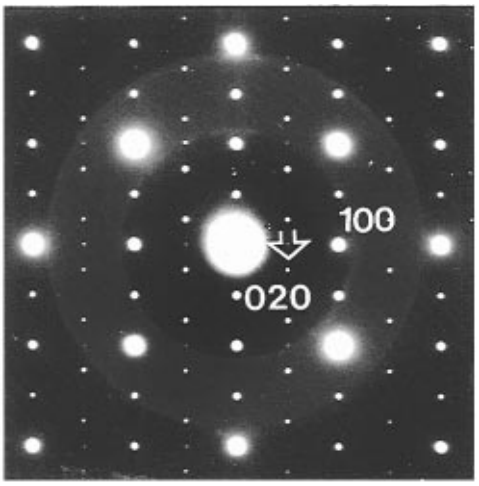


**Figure 2.** Example of [001] ED pattern where a doubling of the $a_0$ parameter is observed. The reflections are indexed in the orthorhombic cell, and the white arrow indicates the extra reflection.

characterize the supercell are clearly visible (Figure 3a). The cell parameters have then been refined to the following values:

$$a_0 = 3.778\ (1)\ \text{Å} \qquad b_0 = 15.244\ (1)\ \text{Å} \approx 4 \times 3.81$$
$$c_0 = 17.677\ (1)\ \text{Å} \approx 2 \times 8.9$$

This definitely establishes that the subcell symmetry is orthorhombic. Note that an orthorhombic cell was also found for $TlSr_2CuO_{4.51}$[2] but with shorter *a* and *b* parameters (3.6607 and 3.7804 Å, respectively) and a longer *c* parameter ($c = 8.9672$ Å).

**HREM and XRD Study: Structural Model for the Long-Range Ordered Oxide $Tl_3(CrO_4)Sr_8Cu_4O_{16}$.** Viewed along [010], the HREM images confirm the "1201" stacking mode of the different layers. The structural features that characterize the superstructure have been studied from the [100] images.

The overall image presented in Figure 4 shows that the extra reflections are correlated to strong variations of the contrast. In this first image, the positions of the cations appear as dark spots and those of the oxygen atoms as bright dots so that the contrast consists mainly in three rows of dark spots, correlated to the Sr, (Tl,-Cr), and Sr rows of the 1201 structure, separated by bright spots correlated to the oxygen atoms of these layers. Between each group of three rows, one row of gray spots is correlated to the $[CuO_2]_\infty$ layers. In such an image, it is clearly visible that, along **b** one dark spot out of four in the thallium layer is replaced by a brighter one, suggesting the substitution of one thallium by a lighter atom. Concomitantly, the four bright spots correlated to the oxygen positions surrounding this atom are highlighted and displaced. Along **c**, in every adjacent 1201 slice, the phenomenon is translated by $b_0/2$, i.e., by $2a_P$, so that a centered image is obtained, in agreement with the A-type symmetry of the orthorhombic cell.

To present the ordering phenomenon, four images of the experimental through-focus series have been selected and given in Figure 5; they have been recorded in the thin edge of the crystal where, moreover, the contrast can be directly compared to that observed for a "normal 1201" structure since the crystal exhibits a small zone where the superstructure is not established.

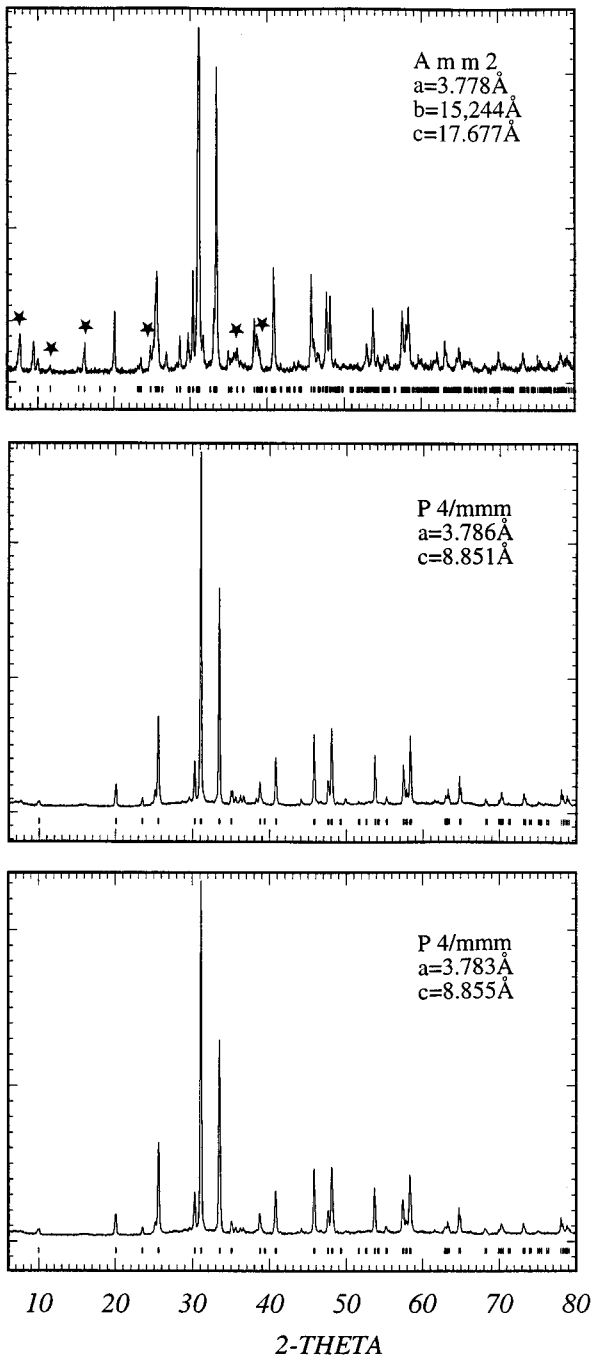


**Figure 3.** Powder X-ray diffraction patterns of the $Tl_{3/4}Cr_{1/4}Sr_{2-x}La_xCuO_5$: (a, top) $x = 0$, (b, middle) $x = 0.05$, and (c, bottom) $x = 0.15$. Reflections marked by stars are due to the supercell.

This "normal 1201" zone is located in the left bottom part of the image where the thallium and copper layers are indicated (the $[SrO]_\infty$ layers being located between the Tl and Cu layers). The contrast modulation due to superstructure is strong for most of the focus values (Figure 5a,c,d) and scarcely visible for few focus values (Figure 5b). These images allow different structural characteristics to be evidenced. In Figure 5a, the heavy atoms appear as dark spots, and one observes that one thallium atom out of four is replaced by a lighter one, and the surrounding oxygen positions are strongly displaced toward this light atom, forming a bright cross. Referring to the nominal composition, this lighter atom is first assumed to be a chromium atom. In this way, the sequence of the cation in the intermediate layer along **b**, would correspond to [−Cr−Tl−Tl−Tl−]. In

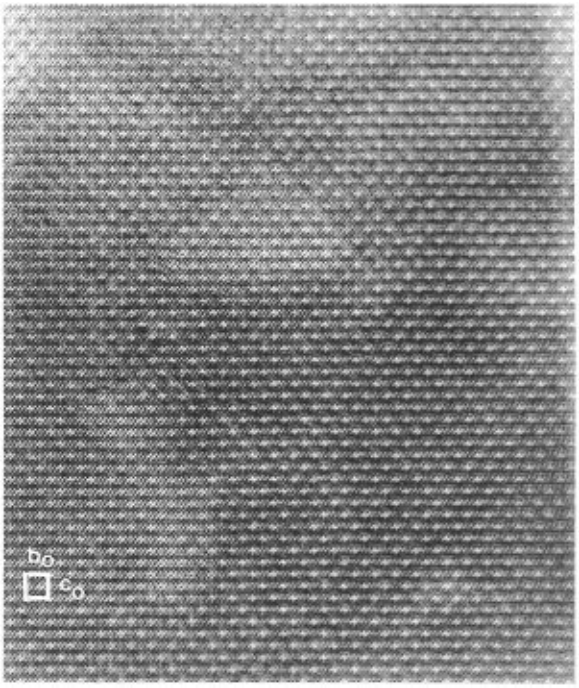


**Figure 4.** [100] HREM image of the ordered phase $Tl_3(CrO_4)Sr_8Cu_4O_{16}$. The strong variation of contrast is observed at the level of the "thallium" layer.

Figure 5c, one observes that the two interatomic Tl−Tl distances are equivalent whereas the Tl−Cr distances are significantly longer. In Figure 5d, the heavy atoms appear as bright dots and the copper positions as the brightest ones. The sequence of three thallium and one lighter atom, which appears as a gray spot, is evidenced as well as the variation in their spacing, and, moreover, one observes that the $[CuO_2]_\infty$ layers are not flat but slightly undulating. An enlarged image recorded for this focus value in the slightly thicker part of the crystal is shown in Figure 6.

Starting from these observations, a structural model can be proposed. Figure 7a presents the cationic arrangement and illustrates that the $[CuO_2]_\infty$ layer shows some waving whereas the mixed "Cr−Tl" layer remains flat. This cationic distribution, directly derived from the HREM observations, suggests the great similarity of this phase with the superconducting oxycarbonates such as $TlSr_2Ba_2Cu_2O_7(CO_3)$ ,[16] in which the carbonate groups and thallium atoms form flat ordered layers interconnected with waving $[CuO_2]_\infty$ layers. In the latter case, the waving of the $[CuO_2]_\infty$ layers allows the size difference between thallium and carbon to be accommodated. In the present phase, this suggests that chromium forms $CrO_4$ tetrahedral groups in such a way that a row of $CrO_4$ tetrahedra alternates with three thallium rows along $\vec{b}$ (Figure 7b). Such a model implies that chromium exhibits the hexavalent oxidation state. This hypothesis is strongly supported by the fact that the reaction is performed under oxygen pressure. The reaction between $Tl_2O_3$ and $Cr_2O_3$ carried out in a sealed

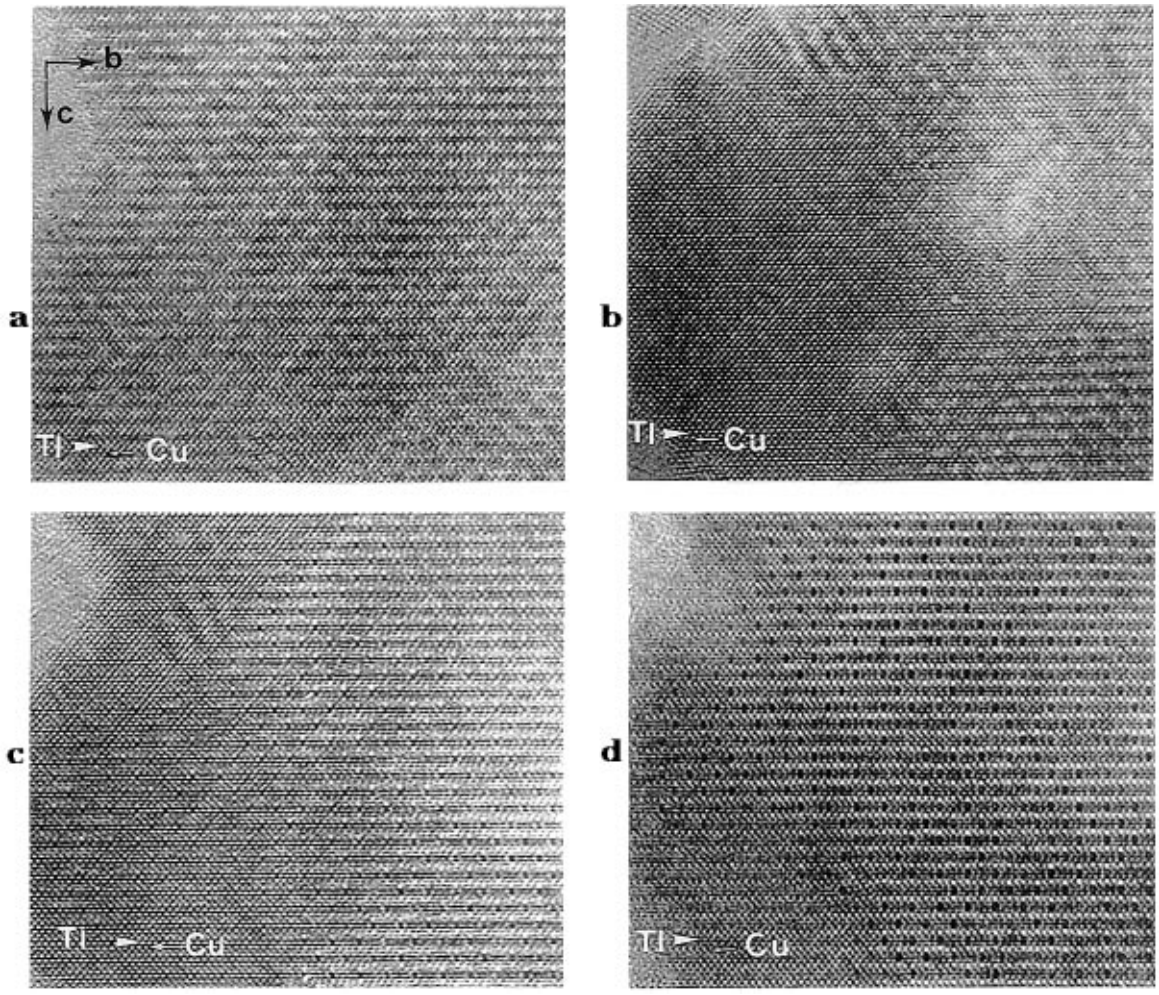


**Figure 5.** Typical images of the experimental through focus series (−5, −15, −35, and −55 nm, respectively). They have been recorded in a thin edge of the crystal, selecting an area where there exists a very small unmodulated zone (left bottom part of the image) to facilitate the interpretation of the contrast and the comparison with a "normal 1201" structure.

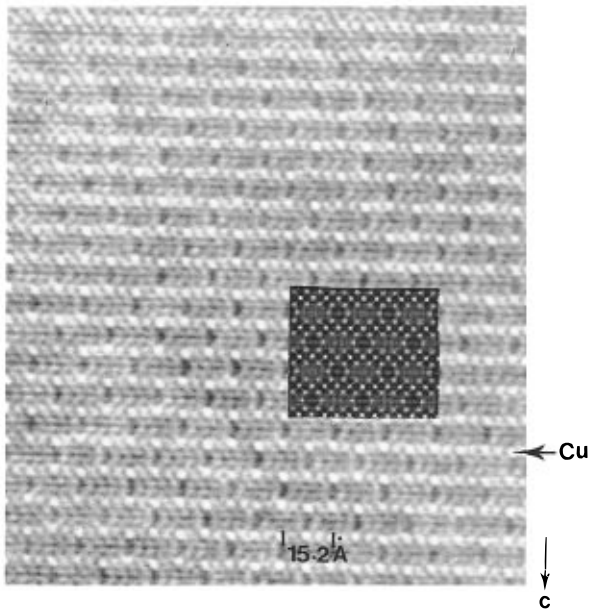


**Figure 6.** Enlarged [100] HREM image of a regular modulated zone and comparison (inset) with the image calculated with the given model in Figure 7b.

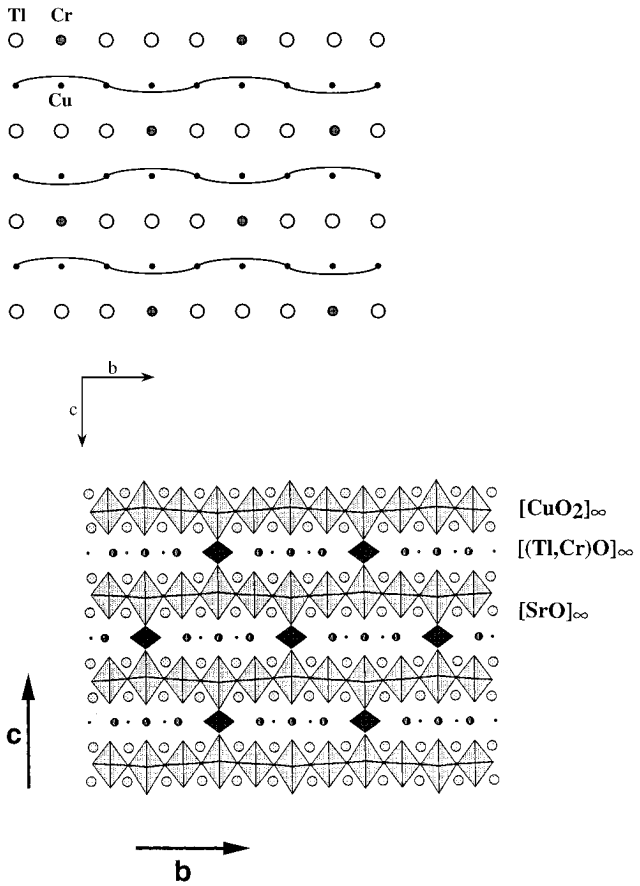


**Figure 7.** Model for the ordered $Tl_3(CrO_4)Sr_8Cu_4O_{16}$ structure (a, top) showing only the copper and mixed ($Tl_3Cr$) layers in order to evidence the Cr ordering and the slight waving of the copper layers (the waving has been exaggerated); (b, bottom) in an idealized representation.

tube confirms this point of view, leading to the formation of the chromate $Tl_2CrO_4$.[17] The tetrahedral coordination

(16) Goutenoire, F.; Hervieu, M.; Maignan, A.; Michel, C.; Martin, C.; Raveau, B. *Physica C* **1993**, *210*, 359.

(17) Carter, R. L.; Margulis, T. N. *J. Solid State Chem.* **1972** , *5*, 75.

**Table 1. Crystallographic Data for $Tl_3(CrO_4)Sr_8Cu_4O_{16}$: Positional Parameters (Only the Positions with Esd Values Have Been Refined)[a]**

| atom | site | *x* | *y* | *z* |
|---|---|---|---|---|
| Tl(1) | 4d | 0 | 0.218 (1) | 0 |
| Tl(2) | 2a | 0 | 0 | 0 |
| Cr(1) | 2a | 0 | 0 | 0.5 |
| Cu(1) | 2a | 0 | 0 | 0.7471 (7) |
| Cu(2) | 2a | 0 | 0 | 0.2529 (7) |
| Cu(3) | 4d | 0 | 0.25 | 0.25 |
| Sr(1) | 4e | 0.5 | 0.121 (4) | 0.1523 (3) |
| Sr(2) | 4e | 0.5 | 0.366 (4) | 0.1474 (3) |
| Sr(3) | 4e | 0.5 | 0.134 (4) | 0.3526 (3) |
| Sr(4) | 4e | 0.5 | 0.378 (4) | 0.3477 (3) |
| O(1) | 2b | 0.5 | 0 | 0.267 (2) |
| O(2) | 2b | 0.5 | 0 | 0.733 (2) |
| O(3) | 4e | 0.5 | 0.25 | 0.25 |
| O(4) | 4d | 0 | 0.125 | 0.2562 (2) |
| O(5) | 4d | 0 | 0.125 | 0.7438 (2) |
| O(6) | 2a | 0 | 0 | 0.102 (2) |
| O(7) | 2a | 0 | 0 | 0.430 (2) |
| O(8) | 2a | 0 | 0 | 0.570 (2) |
| O(9) | 2a | 0 | 0 | 0.898 (2) |
| O(10) | 4d | 0 | 0.25 | 0.108 (1) |
| O(11) | 4d | 0 | 0.25 | 0.892 (1) |
| O(12) | 4e | 0.5 | 0.125 | 0 |
| O(13) | 4e | 0.5 | 0.109 (3) | 0.5 |

[a] Space group: *Amm*2; $a = 3.778$ (1) Å; $b = 15.244$ (1) Å; $c = 17.677$ (1) Å.

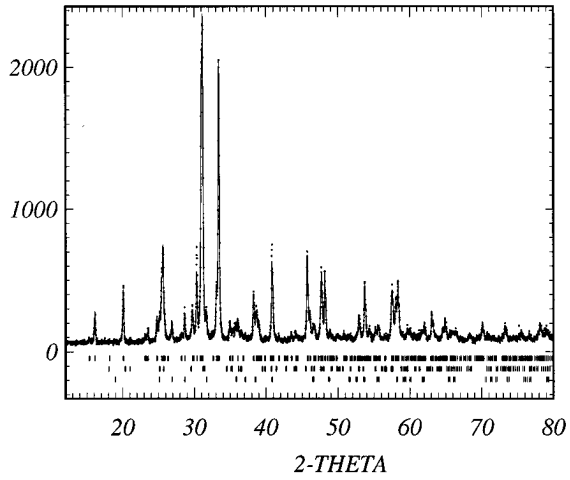


**Figure 8.** Observed and calculated X-ray diffraction patterns for $Tl_3(CrO_4)Sr_8Cu_4O_{16}$. $SrCO_3$ and $Sr_4Tl_2CO_3O_6$ have been considered as impurities.

for chromium is also strongly supported by the HREM observations that evidence a strong displacement of the oxygen atoms toward chromium.

On the basis of this model, idealized atomic positions can be proposed, taking into consideration the size of the different elements. Starting from such positions, structure calculations were performed from powder X-ray data, refining atomic coordinates and fixing the B factors of all the atoms to 1 $Å^2$, owing to the too large number of the independent atoms. The corresponding positional parameters (Table 1), obtained for a $R_I$ factor of 8%, cannot be considered as accurate, especially for the oxygen atoms, but the difference with respect to the ideal "1201" structure is significant especially concerning the displacements of Tl and of the oxygen atoms surrounding these cations within the $[Tl_{3/4}Cr_{1/4}O]_\infty$ layer. The agreement between the observed and calculated pattern (Figure 8) suggests this point of view. A neutron diffraction study is also planned to resolve the structure. The most important confirmation of this structural model, however, deals with the simulated

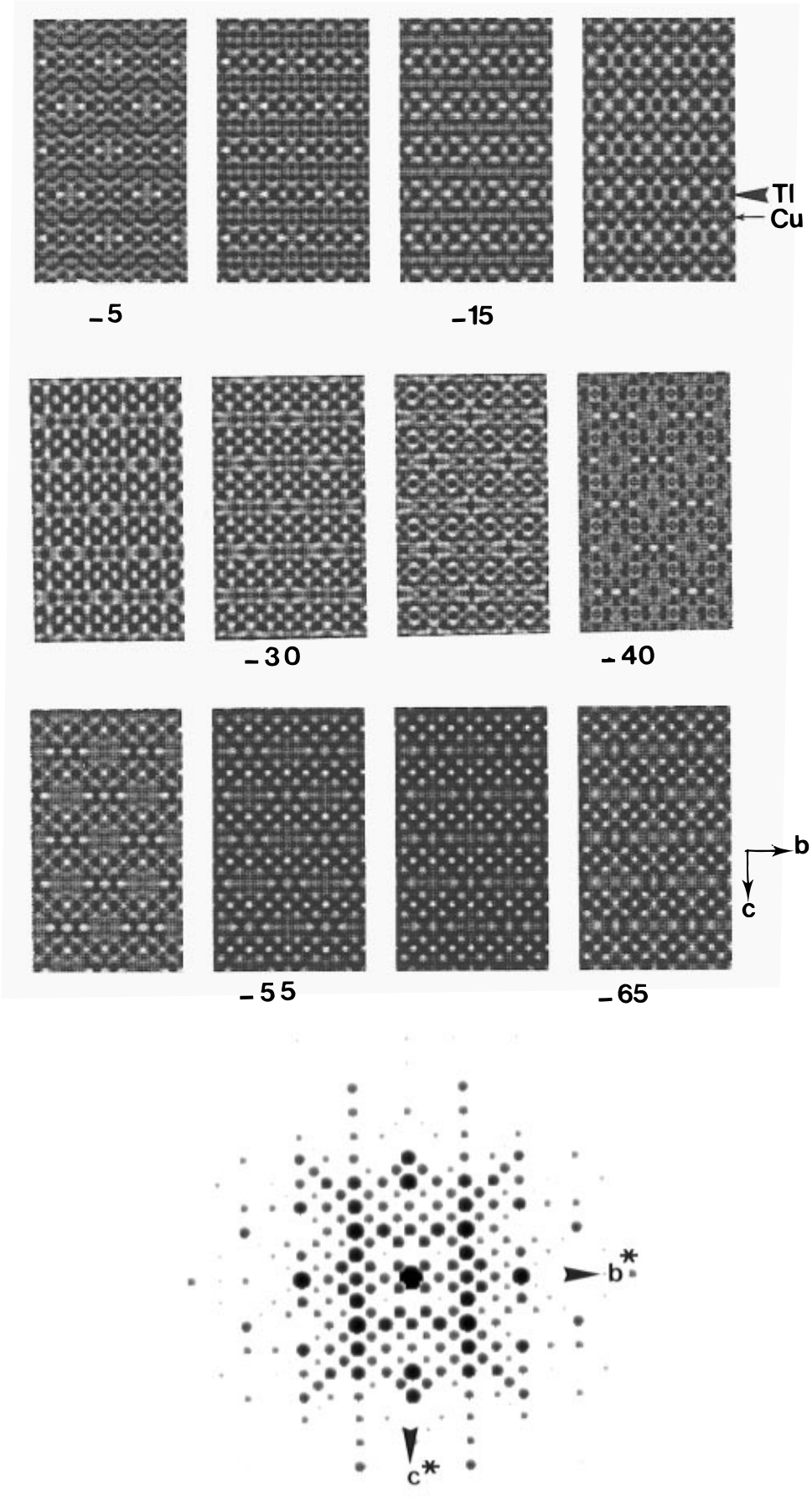


**Figure 9.** (a, top) Calculated images for a crystal thickness of 30 Å; the positional parameters are those given in Table 1. (b, bottom) Calculated [001] E D pattern for this model.

HREM images that have been calculated for different focus values and crystal thickness, using the above atomic coordinates (Table 1). The calculated images for a thickness close to 30 Å (Figure 9a) obtained for focus values of −5, −15, −35, and −55 nm can be easily compared with the observed images of Figure 5a−d,

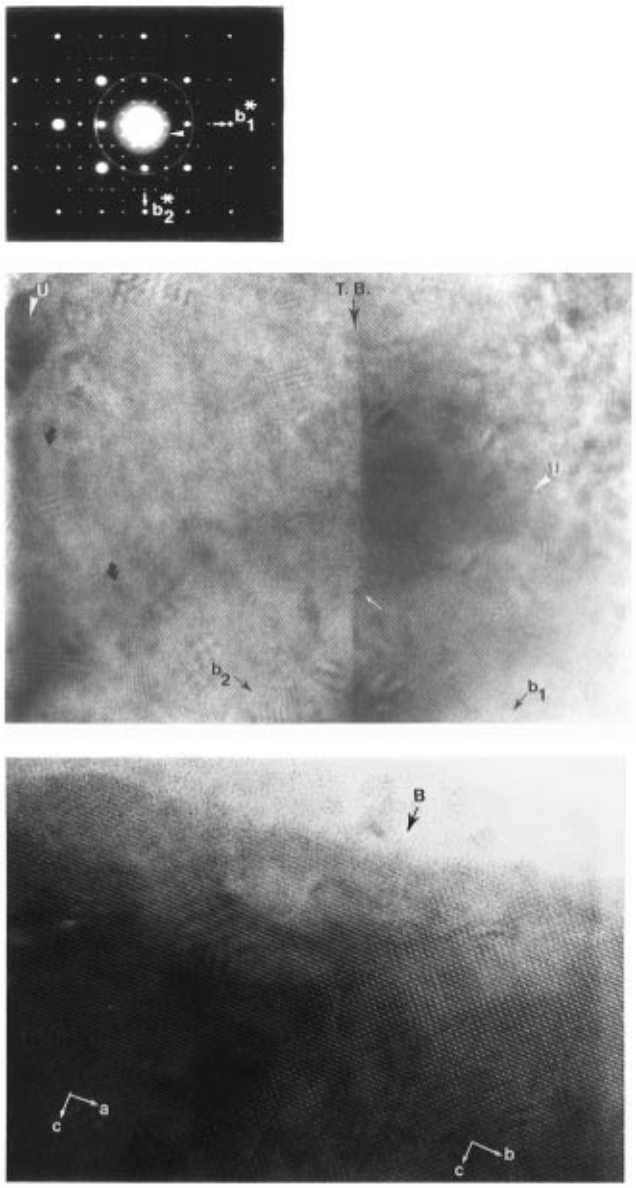


**Figure 10.** Image of a $Tl_3(CrO_4)Sr_8Cu_4O_{16}$ crystal where 90° oriented domains and complex orderings have been observed. (a, top) ED pattern. The two domains are labeled 1 and 2 and the small arrowhead indicates an extra reflection due to the presence of the $2a_0$ structure. (b, middle) The corresponding image. The twin boundary (TB) is straight and locally, the orthorhombic $a_0 \times 2a_P$ superstructure is replaced by an "unmodulated" (U) zone with $a_P \times a_P$ or by complex orderings such as $2a_0 \times 4a_P$ (curved arrows). (c, bottom) Example of a domain boundary (B) viewed along **a** or **b**. Note that the limit between the two domains are not straight.

respectively. The calculated image for a focus value close to −50 nm and a crystal thickness of 60 Å is superposed to the experimental image in Figure 6. The calculated images for the different thicknesses as well as the calculated ED pattern (Figure 9b) confirm the validity of the model.

**Twinning Domains.** As mentioned above, 90° oriented domains are often observed; the [001] images show that the domains are very large and that the twin boundaries (TB) are parallel to the [110] direction of the subcell. One example is shown in Figure 10b, where the **b** axes (marked $\mathbf{b_1}$ and $\mathbf{b_2}$) are perpendicular and the twin boundary, indicated by a large black arrow, is straight. Note that at the level of the small white arrow, the twin boundary is shifted along [110] but the two

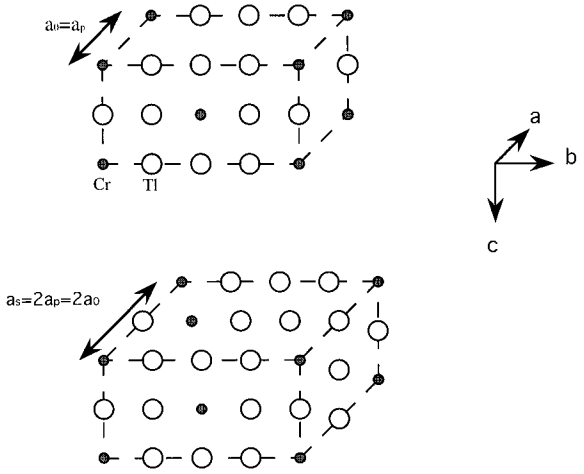


**Figure 11.** Idealized drawing of the Cr and Tl arrangement in (a, top) the $a_0 \times 4a_P \times 2c_{1201}$ and in (b, bottom) the $2a_0 \times 4a_P \times 2c_{1201}$ cells.

domains remain delimited by right angles. Viewed along a perpendicular direction, the boundary (B) is not so sharp because its apparent thickness depends on the crystal thickness (the B is parallel to [110]) but it clearly appears that it is not straight (Figure 10c). These observations imply that within one (001) mixed Tl/Cr layer the boundary is straight and well defined, imposed by strong distortions due to the presence of the chromate group. However, along **c**, the long-range arrangement of the separation between the two domains is not so perfect. Generally, the distribution is highly regular in most of the crystals as presented in Figure 4, but some variations have been observed corresponding to different $Tl_3Cr$ orderings.

In the ED pattern presented in Figure 10a, a third set of reflections is superposed to the two sets corresponding to the two 90° oriented domains. It is similar to the system presented in Figure 2, i.e., it corresponds to a doubling of the $a_0$ parameter. The image (Figure 10b) shows that these weak extra reflections are in fact correlated to the existence of very small areas where the ordering is more complex (some are indicated by curved arrows). Within these areas, the variation of contrast along **b** which is correlated to the ordering of the Tl and Cr is still observed and remains unchanged. However, in the orthorhombic structure (schematic model in Figure 11a), this contrast modulation is translated along **a** by $a_0 = a_P$ , whereas, in the areas in question, it is translated in a first step by $\vec{a}_0 + \vec{b}_0/4$ and afterwards by $\vec{a}_0 - \vec{b}_0/4$ leading to $a' = 2a_0$ (schematical model in Figure 11b).

Figure 12a illustrates the second type of contrast variations. In this image, the chromium sites appear as very bright spots so that their distribution can be easily understood. Different arrangements are observed. The first one is indicated by a large white arrow: at this level, the relative translation along **b** between two adjacent intermediate layers, which would be $2a_P$ and would ensure the centered disposition, is not observed so that the distance between two chromium sites along **c** is locally $c_{1201}$, i.e., $^1/_2c_0$ (Figure 12c). Such an arrangement is rather rare, probably because it is the less favorable from the energy point of view. The second type is indicated by M (for monoclinic) in Figure 12a. Here again, the translation $2a_P$ along **b** is not respected, and instead it is locally just $a_P$. Since this feature is observed over three 1201 units, it involves

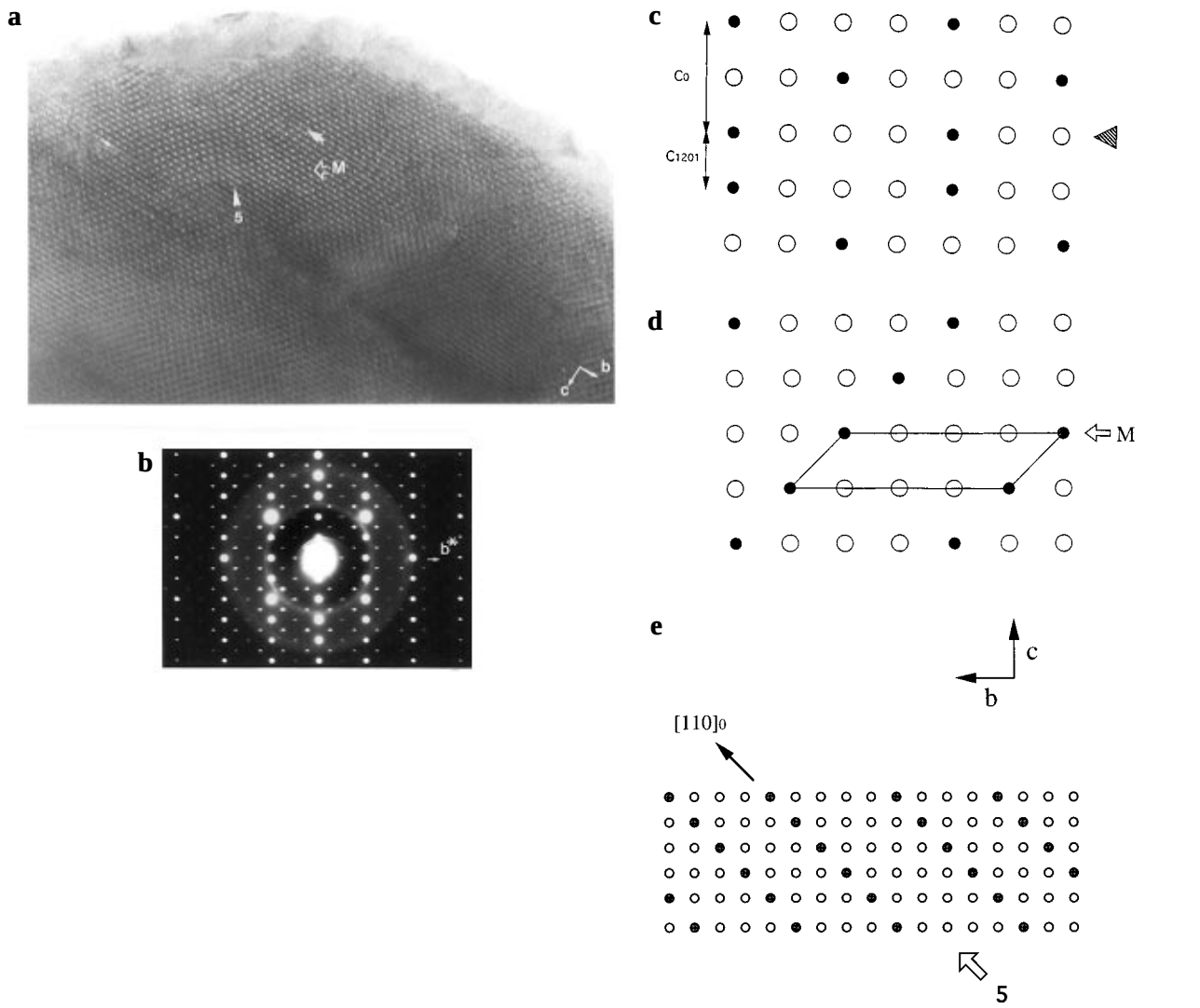


**Figure 12.** Another example of variation of the Tl/Cr distribution in $Tl_3(CrO_4)Sr_8Cu_4O_{16}$. (a) [100] HREM image. The large white arrow in the top part of the image indicates a ($Tl_3Cr$) row where the Cr atoms are at the same level along **c** (a model is proposed in Figure 14a). In the zone labeled M, the $2a_P$ translation along **b** is not respected, involving a monoclinic cell instead of a centered one (a model is proposed in Figure 14b). The white arrowhead shows the local stabilization of a member $m = 5$ (the ordering corresponds to one Cr for every four Tl). (b) The corresponding ED pattern. The $1/m$ value is 0.24, and the reflections are elongated as a result of the disorder. Schematized drawing of the mixed ($Tl_3Cr$) layers with anomalous translation along **b** showing (c) no translation, (d) translation of $a_P$ instead of $2a_P$, and (e) member $m = 5$.

the local formation of a monoclinic cell (Figure 12d). In that part of the image, note that for a 3Tl−1Cr ordering, every possible arrangement of the successive chromium sites along **c** has been observed, with a frequency which seems consistent with the stability of the different arrangements.

**Defective Orderings: $Tl_4Cr$.** The last feature corresponds to a variation of the periodicity along **b**: where it locally becomes $b' = 5a_P$ (indicated by a white arrowhead and 5 in Figure 12a) instead of $4a_P$. This Cr-deficient member is translated by $2a_P$ along **b** so that the chromium sites are aligned along $[110]_0$, as in the normal orthorhombic supercell (Figure 12e). The frequent appearance of these defects is directly detected in the ED patterns, since they result in extra reflections that arise in incommensurate positions. An example is given in Figure 12b. The modulation vector, which is $q^* = 1/mb^* + {}^1/_2c^*$ with $1/m = 0.25$ in the perfect orthorhombic structure, is characterized by $1/m = 0.24$. This small difference can be easily observed from the elongated shape of the $(0kl)_0$ reflections with $l = 2n$ and $k = 2n + 2$.

**Lanthanum Doping.** The substitution of lanthanum for strontium is recognized as one route to stabilize the "1201" structure as previously shown for the superconductor $TlSr_{2-x}La_xCuO_{5-\delta}$.[18,19]

To understand the influence of chromium and lanthanum upon the stabilization of the "1201" structure, we have tried to substitute partially lanthanum for strontium and simultaneously chromium for thallium in $TlSr_2CuO_{5-\delta}$. A pure phase could be synthesized for the nominal composition $Tl_{0.8}Cr_{0.2}Sr_{1.95}La_{0.05}CuO_{6.47}$. The EDS analysis performed on numerous crystals confirms that the cationic composition of each of them does not vary and is close to the nominal one. The XRD and ED patterns of this phase show a spectacular difference with respect to the copper oxychromate $Tl_3(CrO_4)Sr_8Cu_4O_{16}$. Indeed one observes that all the extra reflections in the powder XRD patterns have disappeared (Figure 3b) so that it can be indexed in a tetragonal cell with $a = 3.786$ (1) Å and $c = 8.851$ (1) Å.

(18) Subramanian, M. A. *Mater Res. Bull* **1990**, *25*, 191.
(19) Huvé, M.; Michel, C.; Martin, C.; Hervieu, M.; Maignan, A.; Provost, J.; Raveau, B. *Physica C* **1991**, *179*, 214.

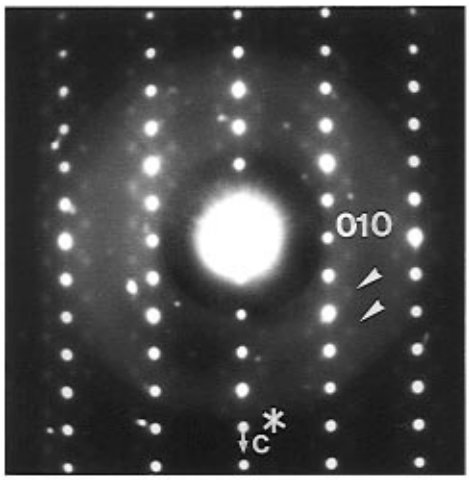


**Figure 13.** [100] ED pattern of a $Tl_{3/4}Cr_{1/4}Sr_{1.95}La_{0.05}CuO_5$ crystal . The extra reflections are very weak, and $1/m$ is close to 0.22.

The ED patterns of most of the crystals exhibit only weak extra reflections lying in incommensurate positions, as illustrated for example in Figure 13, where the incommensurate satellites are scarcely visible ($q = 0.22$). Only few crystals still exhibit the ordered structure, which are at the limit of the lanthanum detection.

These results clearly establish that a small doping by lanthanum destroys the long-range ordering between chromium and thallium and favors tetragonal symmetry. The origin of this difference is still unexplained to date, and it may be related to a change of the oxidation state and coordination of chromium.

**Superconducting Properties.** The $\chi(T)$ curves of the two samples, the pure strontium and the 0.05-La-doped phases, are given in Figure 14. The as-synthesized copper oxychromate $Tl_3(CrO_4)Sr_8Cu_4O_{16}$ exhibits a clear transition at 21 K (curve a) with a rather significant superconducting volume fraction (40% at 5 K), whereas for the La-doped phase one observed a very low diamagnetic volume fraction (less than 2%, curve b), with a very broad transition ($T_c$(onset) $\approx$ 20 K).

Annealing in a reducing atmosphere (90% Ar, 10% $H_2$) at 280 °C shows that the as-synthesized samples are overdoped. The $T_c$ of $Tl_3(CrO_4)Sr_8Cu_4O_{16}$ is increased up to 34 K by annealing (curve c), the superconducting volume fraction being maintained at ≈40%. The La-doped sample is also improved by annealing (curve d), but the transition is still very broad, and the superconducting volume fraction reaches 20% at 5 K.

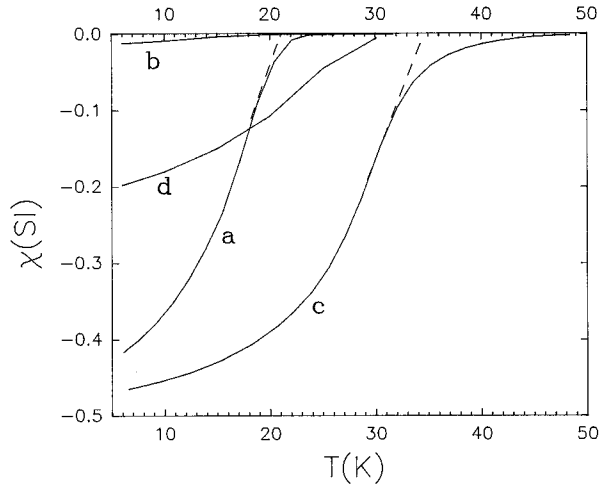


**Figure 14.** $\chi(T)$ curves for $Tl_3(CrO_4)Sr_8Cu_4O_{16}$ (a) as-synthesized and (c) $Ar-H_2$ annealed and $Tl_{3/4}Cr_{1/4}Sr_{1.95}La_{0.05}CuO_5$ (b) as-synthesized and (d) $Ar-H_2$ annealed.

## Concluding Remarks

A long-range ordering between thallium and transition element has been shown for the first time in thallium cuprates. This "1201" ordered phase can be interpreted as copper oxychromate with the formula $Tl_3(CrO_4)Sr_8Cu_4O_{16}$, characterized by an ordered replacement of one Tl row out of four by one row of $CrO_4$ tetrahedra. This behavior is very similar to that observed for copper oxycarbonates that are built up of rows of $CO_3$ groups replacing the thallium rows. Such a similarity suggests the possible existence of other members with the general formulation $Tl_{m-1}CrO_4Sr_{2m}Cu_mO_{5m-4}$, corresponding to the ordered replacement of one thallium row of m by one row of $CrO_4$ tetrahedra. The present compound represents the member $m = 4$, whereas the superstructure "$b = 5a_p$" observed as a local defect by HREM corresponds to the $m = 5$ member. The effect of a small La doping is remarkable since it involves a sudden transition from an ordered orthorhombic cell to a classical tetragonal "1201" cell without long-range ordering. The road is open for the research of other superconducting copper oxychromates.

**Acknowledgment.** The authors thank V. Hardy (Crismat) for magnetic measurements. They are grateful to the European Communiy for financial support.

CM950473I